



CHALMERS
UNIVERSITY OF TECHNOLOGY

Vertical transport of buoyant microplastic particles in the ocean: The role of turbulence and biofouling

Downloaded from: <https://research.chalmers.se>, 2025-03-09 00:35 UTC



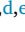


Citation for the original published paper (version of record):

Sugathapala, T., Capuano, T., Brandt, L. et al (2025). Vertical transport of buoyant microplastic particles in the ocean: The role of turbulence and biofouling. *Environmental Pollution*, 369. <http://dx.doi.org/10.1016/j.envpol.2025.125819>

N.B. When citing this work, cite the original published paper.



Vertical transport of buoyant microplastic particles in the ocean: The role of turbulence and biofouling

Thisal Mandula Sugathapala ^a ,* , Tonia Capuano ^b , Luca Brandt ^{c,d,e} , Daniele Iudicone ^f , Gaetano Sardina ^a 

^a Department of Mechanics and Maritime Sciences, Chalmers University of Technology, Gothenburg, 41296, Sweden

^b Department of Oceanography & International Centre for Ocean Governance (ICOG), University of Dhaka, Dhaka, 1000, Bangladesh

^c FLOW, Department of Engineering Mechanics, KTH, Stockholm, Sweden

^d Department of Energy and Process Engineering, Norwegian University of Science and Technology (NTNU), Trondheim, Norway

^e Department of Environment, Land, and Infrastructure Engineering, Politecnico di Torino, Corso Duca degli Abruzzi 24, Turin, 10129, Italy

^f Stazione Zoologica Anton Dohrn, Villa Comunale, Naples, 80121, Italy

ARTICLE INFO

Keywords:

Biofouling
Microplastics
Random walk models
Lagrangian particle tracking

ABSTRACT

This study investigates the interactions between turbulence and biofouling and their influence on the vertical transport of buoyant microplastic particles in a marine environment. We explore the sinking characteristics for a range of particle densities and sizes, focusing on comparing laminar and turbulent flows with diffusivity profiles typical of the North Pacific Ocean. The results show the existence of three flow regimes based on the relative importance between turbulent fluctuations and biofilm growth. The biofouling process determines the vertical motion of microplastic particles of sizes in the millimeter range. In contrast, particles in the micrometer range are found to follow flow trajectories without any significant influence from biofouling. We observe that turbulence, on average, promotes the beginning of the vertical particle settling; for example, a high-density polyethylene particle of 1 mm in size has an average settling onset of 10 days in the presence of turbulence, while in its absence, this occurs in 19 days. We also show that turbulence causes buoyant microplastic particles smaller than 0.1 mm to spend their entire lifespan underwater. Finally, the probability distributions for particle size after 100 days in the ocean reveal that particle density strongly influences the biofilm thickness for particles larger than 10 μm . We will discuss the implications of these results for tracking the motion of microplastic particles in large-scale regional or global numerical models.

1. Introduction

Mass production of synthetic polymers, more commonly known as plastic, first began in the early 1950s (United Nations Environment Programme, 2021) and has steadily increased to reach an annual output of 390.7 million tons by 2021 (Plastic Europe, 2022). Global estimates for plastic waste leaking into aquatic ecosystems have reached 23 million tons by 2016, and it is predicted to increase to at least 53 million tons by 2030 (Borrelle et al., 2020). Over time, plastic waste breaks down into smaller pieces due to weathering and fragmentation (Andrady, 2022). Such particles of sizes between 5 mm and 0.1 μm are defined as microplastics (Hidalgo-Ruz et al., 2012; Li et al., 2023). The accumulation of microplastics in the ocean raises concerns about their potential threat to the marine ecosystem (Cole et al., 2011).

Consequently, extensive research is currently being carried out to investigate the fate of microplastics in the marine environment. Numerical simulations are essential to these investigations as they can capture

the dynamic behavior of microplastic particles. Such models aim to have predictive capabilities for identifying potential accumulation regions (Zhang, 2017). Numerical simulations to model microplastic transport can be broken down into Eulerian models, Lagrangian particle tracking models, or hybrid models (Shamskhany and Karimpour, 2022). The Eulerian approach accounts for fluid motion with a fixed reference frame in space (Alosairi et al., 2020). On the other hand, Lagrangian particle tracking models utilize a moving frame of reference that follows the particle (van Sebille et al., 2018). Particle tracking models have been shown to have numerous advantages over the traditional Eulerian approach when considering particle dynamics (Hunter, 1987). However, hydrodynamic details, such as the ocean's velocity fields, ocean depths, and wind data, are provided in Eulerian format from Ocean General Circulation Models (OGCMs). Therefore, most existing

* Corresponding author.

E-mail address: thisal@chalmers.se (T.M. Sugathapala).

<https://doi.org/10.1016/j.envpol.2025.125819>

Received 1 November 2024; Received in revised form 27 January 2025; Accepted 5 February 2025

Available online 13 February 2025

0269-7491/© 2025 The Authors. Published by Elsevier Ltd. This is an open access article under the CC BY license (<http://creativecommons.org/licenses/by/4.0/>).

microplastic tracking models adopt a hybrid Lagrangian-Eulerian approach, combining Lagrangian particle tracking with Eulerian-based oceanographic models (Iwasaki et al., 2017; Daily and Hoffman, 2020; Xue et al., 2018). Such studies have been extensively carried out on a global scale (Potemra, 2012) as well as on regional scales, such as in the Mediterranean Sea (Mansui et al., 2015; Liubartseva et al., 2018; Capuano et al., 2024).

While hybrid models are the most suitable method to investigate the flow of microplastic particles in water bodies, Lagrangian particle tracking models are more convenient for gaining fundamental insights into how different physical and biological processes interact with each other and influence the size, density, and hence, the motion of microplastic particles. Such models use parameterized equations to represent numerous physical and biological processes such as beach wash-off, sea-floor deposition, re-suspension, degradation, and biofouling (Bigdeli et al., 2022).

In particular, of interest here, biofouling can be defined as the buildup of micro-organisms on the surface of plastic particles, affecting their buoyancy and hydrophobicity (Kaiser et al., 2017). It is a crucial phenomenon to accurately capture in microplastic tracking software (Van Melkebeke et al., 2020). This can be attributed to its influence on the sinking rates of buoyant microplastic particles that are supposed to float on the ocean's surface (Fazey and Ryan, 2016). With over 49% of manufactured plastics being buoyant and only 1% of the plastic entering the ocean found to float on the surface, biofouling is a critical process to consider when investigating the fate of the so-called "lost" plastic in the ocean (Cózar et al., 2014).

Different approaches are currently used among microplastic debris tracking software to account for biofouling. The most common method is to assume the biofilm thickness is increasing at a constant rate, as implemented by TrackMPD (Jalón-Rojas et al., 2019) and CAMPSim-3D (Pilechi et al., 2022). The most comprehensive and accurate biofouling modeling approach was presented by Kooi et al. (2017), hereafter called the Kooi model, and its influence on the vertical transport of microplastics was explored with a laminar flow assumption. Two follow-up publications connected the Kooi model to a hydrodynamic model called NEMO-MEDUSA 2.0 ORCAO083-N06 output (Fischer et al., 2022; Lobelle et al., 2021). Lobelle et al. (2021) improved the growth term of the biofouling differential equation by considering nutrient limitations by nitrate, silicon, and iron. Fischer et al. (2022) also improved upon Kooi's model by accounting for vertical mixing due to turbulence and adding two new biofilm loss terms due to explicit grazing and viral lysis. While it is clear that these recent studies show a realistic approach to account for biofilm growth in the ocean, little is understood about how turbulence interacts with biofouling growth.

Therefore, this study extends the original Kooi model to capture the interactions between turbulence and biofouling processes and investigates their influence on the vertical transport of biofouled buoyant microplastic particles. In particular, we develop a new Lagrangian biophysical particle tracking model to capture the intermittent nature of turbulence in biophysical particle tracking models, analyze the role of turbulence in modifying the biofouling rate of buoyant microplastic particles, and investigate the impact of turbulence on particle motion and settling onset.

2. Materials and methods

2.1. Particle tracking model

Similar to Fischer et al. (2022), we use the concept of eddy diffusivity (K) to capture the influence of turbulence diffusion on particle motion. To generate the diffusivity profile as a function of depth z , we use the K -profile parameterized equation given below (Bouffadel et al.,

2020).

$$K(z) = \left(\frac{\kappa u_{*w} \theta}{\phi} \right) (|z| + z_0) \left(1 - \frac{|z|}{MLD} \right)^2 \quad (1)$$

In Eq. (1), the mixed layer depth (MLD) is highly dependent on the location, κ is the von Kármán constant, u_{*w} is the friction velocity of the sea's surface, ϕ is the stability function of the Monin-Obukhov boundary layer theory, and θ is the Langmuir circulation enhancement factor. We calculate the roughness scale of turbulence (z_0) using Eq. (2) as shown below (Zhao and Li, 2019):

$$z_0 = 3.5153 \times 10^{-5} \left(\frac{\beta_* u_{*a}}{u_{10}} \right)^{-0.42} \frac{u_{10}^2}{g} \quad (2)$$

where β_* is the wave age, u_{*a} is the friction velocity for air, u_{10} is the wind speed at a height of 10 m above sea level, and g is the gravitational constant. With a known diffusivity profile, the next step is selecting a suitable random walk model. Eqs. (3) and (4) can be derived as the appropriate random walk model to describe particle motion in nonuniform diffusivity fields (Visser, 1997; Hunter et al., 1993):

$$T_{stoc} = R \left[\frac{2K(z_n + \frac{1}{2}K'(z_n)\Delta t)}{r\Delta t} \right]^{\frac{1}{2}} \quad (3)$$

$$z_{n+1} = z_n + K'(z_n)\Delta t + T_{stoc}\Delta t + w_p\Delta t \quad (4)$$

where R is a normally distributed random weight with a mean of zero and a variance of r . Eq. (4) consists of three contributions to particle motion which include a deterministic term representing the gradient of diffusivity ($K' = dK/dz$), a random term (T_{stoc}), and an intrinsic motion term (w_p). The intrinsic motion term accounts for the settling, sinking, or swimming velocity of the considered particle, which in the present study, represents the settling velocity caused by the biofouling process. This settling velocity is defined as:

$$w_p = - \left[\frac{\rho_{tot} - \rho_{sw,z}}{\rho_{sw,z}} g \omega_* v_{sw,z} \right]^{\frac{1}{3}} \quad (5)$$

where ρ_{tot} is the total density of the biofouled microplastic particle, $\rho_{sw,z}$ is the density of sea water, $v_{sw,z}$ is the kinematic viscosity of sea water, and ω_* is the dimensionless settling velocity. ω_* is based on the dimensionless particle diameter D_* , calculated using the model proposed by Dietrich for spherical particles (Dietrich, 1982):

$$\omega_* = \begin{cases} 1.71 \times 10^{-4} D_*^2, & \text{for } D_* < 0.05 \\ -3.76715 + 1.92944 \log D_* - 0.09815 (\log D_*)^2 \\ -0.00575 (\log D_*)^3 + 0.00056 (\log D_*)^4, & \text{for } 0.05 \leq D_* \leq 5 \times 10^9 \end{cases} \quad (6)$$

$$D_* = \frac{(\rho_{tot} - \rho_{sw,z})gD_n^3}{\rho_{sw,z}v_{sw,z}^2} \quad (7)$$

where D_n is the nominal diameter. In this work, we will only consider the case of spherical particles. In the case of complex particle shapes, a correction to the previous expression in terms of a Corey shape factor can be found in Francalanci et al. (2021). Further details on the implementation of this expression can be found in Kooi et al. (2017). For surface boundary conditions, we adopt a randomly mixed layer model, as recommended by Ross and Sharples (2004):

$$z_{n+1} = z_{pdt}H \quad \text{if } z_{n+1} < z_t \quad (8)$$

where H is a random weight uniformly distributed between 0 and 1. The depth z_{pdt} is defined as the maximum possible displacement for a particle from the ocean surface and is defined using Eq. (9), where R_{max} is the maximum numerical value for the random process R .

$$z_{pdt} = K'(z_{pdt})\Delta t + R_{max} \left[\frac{2K(z_{pdt} + \frac{1}{2}K'(z_t)\Delta t)}{r} \right]^{\frac{1}{2}} \quad (9)$$

This approach will create a randomly mixed layer for all particles within a distance z_{pdt} from the ocean surface. To compare the similarity between particle motion in turbulent and laminar flow, we adopt the Pearson correlation coefficient (P):

$$P = \frac{\sum_{i=1}^i (z_t^i - \bar{z}_t)(z_l^i - \bar{z}_l)}{\sqrt{\sum_{i=1}^i (z_t^i - \bar{z}_t)(z_t^i - \bar{z}_t) \sum_{i=1}^i (z_l^i - \bar{z}_l)(z_l^i - \bar{z}_l)}} \quad (10)$$

where z_t^i and z_l^i are the particle locations with respect to timestep i for a turbulent and laminar flow, while \bar{z}_t and \bar{z}_l are their respective average values.

2.2. Biofouling model

As mentioned before, we describe the biofilm gain and loss terms using the Kooi model. The differential equation that captures the rate of change of attached algae (A) is given by the following expression:

$$\frac{dA}{dt} = \frac{\beta_A A_A}{\gamma_{pl}} + \mu_A A - m_A A - + Q_{10}^{\frac{T-20}{10}} R_A A \quad (11)$$

where dA/dt is defined as the biofouling rate. The first term on the right-hand side of Eq. (11) represents the increase in biofilm thickness due to collision between algae and microplastic particles where β_A is the collision rate, A_A is the ambient algae concentration, and γ_{pl} is the plastic particle's surface area. The second term considers the growth of attached algae (μ_A) being limited by temperature and light while assuming sufficient nutrient availability. The third and fourth terms approximate biofilm loss due to grazing mortality and respiration, respectively. A constant mortality (m_A) of 0.39 d^{-1} and a constant respiration rate (R_A) of 0.1 d^{-1} with a Q_{10} value of 2 are utilized, similar to Kooi et al. (2017). The only change we make to the original Kooi model is to improve the biofilm growth due to collision in the presence of turbulence. In Kooi's model, the biofouling rate resulting from collision frequency comprises three components: Brownian motion ($\beta_{A,Brownian}$), differential settling/sedimentation ($\beta_{A,settling}$), and constant advective shear ($\beta_{A,shear}$). Mathematically, this is expressed as:

$$\beta_A = \beta_{A,Brownian} + \beta_{A,settling} + \beta_{A,shear} \quad (12)$$

However, the constant advective shear term is only valid under the assumption of laminar flow. Therefore, we replace this term with a more appropriate turbulent shear term (Burd and Jackson, 2009).

$$\beta_{A,shear} = 1.3 \left(\frac{\epsilon_{sw,z}}{v_{sw,z}} \right)^{\frac{1}{2}} (r_{tot} + r_A)^3 \quad (13)$$

where $\epsilon_{sw,z}$ is the turbulence dissipation rate at depth z . We estimate $\epsilon_{sw,z}$ from the diffusivity profile using Osborn's model (Osborn, 1980).

$$K(z) = \Gamma \left(\frac{\epsilon_{sw,z}}{N_{bv}^2} \right) \quad (14)$$

In the above, Γ is called the efficiency factor, which represents the ratio between the rate of increase of potential energy to the rate of decrease in kinetic energy in turbulent flows (Thorpe, 2007). N_{bv} is the mean buoyancy frequency, also known as the Brunt-Väisälä frequency, defined using the following expression:

$$N_{bv}^2 = \frac{g}{\rho_{sw,z}} \left| \left(\frac{d\rho}{dz} \right)_{sw,z} \right| \quad (15)$$

In Eq. (15), we use the absolute value of the density gradient ($d\rho/dz$) to prevent numerical instabilities arising from negative density gradients. Eqs. (14) and (15) provide a means of approximating $\epsilon_{sw,z}$ from diffusivity profiles and hence estimating the influence of $\epsilon_{sw,z}$ on any biophysical phenomenon. However, this is an estimate of the mean $\epsilon_{sw,z}$ but turbulence in nature is intermittent (Watteaux et al., 2019), meaning that the dissipation fluctuations are not rare and can be several times larger than their mean value (Isern-Fontanet and Turiel, 2021). To capture the intermittent nature of $\epsilon_{sw,z}$, we resort

to the stochastic turbulence dissipation model by (Pope and Chen, 1990), hereafter called the Pope and Chen model. This is based on the variable $\chi(t)$, generated by an Ornstein-Uhlenbeck process, i.e, solving the following differential equation:

$$d\chi = -(\chi - \bar{\chi}) \frac{dt}{T_\chi} + \left(\frac{2\sigma_\chi^2}{T_\chi} \right)^{\frac{1}{2}} dW \quad (16)$$

where W is a Wiener process with zero mean and variance dt . The order of magnitude of the turbulent dissipation is given by the relationship $\chi(t) = \ln(\epsilon/\bar{\epsilon})$, which has a variance of σ_χ^2 with an integral time scale of T_χ . In addition, $\bar{\chi}$ can be shown to be equal to $-1/\sigma_\chi^2$ (Pope and Chen, 1990). Empirical expressions for σ_χ and T_χ have been developed in a follow-up study by Yeung et al. (2006):

$$\sigma_\chi = A + \frac{3\mu}{2} \ln Re_\lambda \quad (17)$$

$$T_\chi = T_0 \left(0.055 + \frac{3.55}{Re_\lambda^{0.7}} \right) \quad (18)$$

as a function of the Taylor scale Reynolds number (Re_λ) (Yeung et al., 2006). T_χ is normalized by the integral time scale (T_0) which is given by:

$$T_0 = \frac{3}{2} \left(\frac{\sigma_U^2}{\bar{\epsilon}} \right) \quad (19)$$

where σ_U is the variance of velocity (Lamorgese et al., 2007). Under the assumption of isotropic turbulence, Eq. (19) is simplified to:

$$T_0 = \left(\frac{3}{20} \right)^{\frac{1}{2}} Re_\lambda \tau_k \quad (20)$$

where τ_k is the Kolmogorov time scale (Watteaux et al., 2019).

$$\tau_k = \left(\frac{\nu}{\bar{\epsilon}} \right)^{\frac{1}{2}} \quad (21)$$

To implement the Pope and Chen model, the local flow Re_λ is estimated based on the Taylor microscale (λ):

$$\lambda = \left(\frac{10\nu k}{\epsilon} \right)^{\frac{1}{2}} \quad (22)$$

where k is the turbulent kinetic energy (Pope, 2000). An approximation for k is necessary not only to calculate λ , but also to calculate flow velocity $U = (2 \times k)^{0.5}$, needed to find the local flow Re_λ . The proposed model uses a $k-l$ model that parameterizes the dependence of K on the mixing length scale l and k (Baas et al., 2008).

$$K(z) = l \sqrt{k} \quad (23)$$

The model shown in Eq. (23) was first implemented for an oceanographic case by Gaspar et al. (1990) This closure is highly dependent on accurately capturing l , and several models have been proposed over the years (Canuto et al., 2001). In this study, we adopt the length scale proposed by Deardorff (1980) for stable stratification conditions, as expressed in Eq. (24):

$$l = c_\phi \frac{\sqrt{k}}{N_{bv}} \quad (24)$$

where the mixing constant (c_ϕ) is assumed as $c_\phi = \sqrt{2}$ with the first order approximation proposed by Blanke and Delecluse (1993), which is valid in a stably stratified region. Additional numerical values necessary to implement the model described above can be found in Tab. S1 and the diffusivity profile is visualized in Fig. S1. We have also implemented a sun-tracking model to evaluate the impact of dynamic day lengths with higher latitudes on particle settling dynamics. Further details on this model, along with corresponding results, can be found in supplementary data (Text S1, Fig. S3, and Fig. S4).

2.3. Simulation parameters

We carry out all simulations with profiles from Kooi et al. (2017) for the North Pacific Ocean near Hawaii. We use Eq. (1) to recreate the mean diffusivity profile for the North Pacific Subtropical Gyre as shown by Fischer et al. (2022). Although the presented mathematical framework allows for incorporating variations in space and time, the current implementation employs static profiles. By doing so, we isolate specific variables, enabling a more precise and focused analysis of how each variable influences particle behavior. Based on sensitivity studies, we set the total time duration to 100 days, sufficient to capture the distinct flow features examined in this study adequately. We use a time step (Δt) of 1 s when the Pope and Chen model is activated and 100 s otherwise. Both timesteps are found to be adequate in terms of having sufficient numerical accuracy at minimum computational cost. We selected three commonly used types of plastics, Polypropylene (PP), Low-density polyethylene (LDPE), and High-density polyethylene (HDPE) with particle densities of 840 kg/m³, 920 kg/m³, and 960 kg/m³, respectively (Kooi et al., 2017). Particle sizes, expressed as diameters, ranged from 5 mm to 0.1 μ m. To prevent numerical instabilities, we set minimum values of $1 \times 10^{-6} \text{ m}^{-2} \text{ s}^{-1}$ for $K(z)$, $1 \times 10^{-10} \text{ W/kg}$ for $\bar{\epsilon}$, and both a minimum value of $1 \times 10^{-14} \text{ W/kg}$ and a maximum value of $1 \times 10^{-4} \text{ W/kg}$ for ϵ . The numerical algorithm was developed in Fortran and incorporated MPI (Message Passing Interface) for parallel computing.

3. Results and discussion

3.1. Biofouling rate

We first investigate how incorporating a detailed turbulence dissipation model captures the intermittent nature of ϵ , influences the turbulent shear experienced by a particle, and consequently affects biofilm growth. For various particle motions, we find that the mean dissipation $\bar{\epsilon}$ ranges from $1 \times 10^{-6} \text{ W/kg}$ to $1 \times 10^{-10} \text{ W/kg}$, while the dissipation ϵ varies between $1 \times 10^{-4} \text{ W/kg}$ and $1 \times 10^{-14} \text{ W/kg}$. These turbulence dissipation rates have been previously reported in field measurements (Whalen, 2021; Thorpe, 2005; Peters and Gregg, 1988) and are utilized in global ocean models (Pearson and Fox-Kemper, 2018). Fig. 1 illustrates the time history of the biofouling rate (dA/dt) experienced by a single 1 μ m LDPE particle under two scenarios: a model expressing the shear as a function of the mean dissipation rate (a), and the detailed model by Pope and Chen (b). In the simpler model, the biofouling rate reached a maximum value of $280 \text{ m}^{-2} \text{ s}^{-1}$. On the other hand, the inclusion of the Pope and Chen model increases the peak biofouling rate to about $1897 \text{ m}^{-2} \text{ s}^{-1}$. The data in Fig. 1 correspond to a single particle trajectory, illustrating a typical intermittent signal of the shear experienced by a particle in turbulence. The values of the biofouling rates vary for different particles with different sizes. However, the qualitative behavior remains the same. For the remainder of this manuscript, the data under turbulent conditions are ensemble-averaged over a sufficiently large sample of distinct particle trajectories.

In Fig. 2, we compare the contribution from shear towards the biofouling rate ($\beta_A A_A / \gamma_{pl}$) (a), and we quantify the biofilm thickness using the mean number of attached algae per unit area (b), as a function of particle size under different turbulent and laminar models. In both plots, mean values are averaged over the final 10 days of simulations. The two different turbulent shear expressions are compared where the turbulent shear is calculated using Pope and Chen model (red lines/symbol), and using the average dissipation $\bar{\epsilon}$ (green lines/symbols). For laminar flow (purple lines/symbols), we apply a constant shear rate of $1.7 \times 10^5 \text{ day}^{-1}$ following Kooi et al. (2017).

Fig. 2(a) shows that due to this approximation, the shear biofouling rate in laminar flow is much higher except for the smaller particles. Under turbulent conditions, the biofouling rate due to turbulent shear

calculated using the Pope and Chen model is lower than $\bar{\epsilon}$, especially for particles larger than 0.1 mm. However, for such large particles, it is shown that the number of attached algae (Fig. 2(b)) is similar for all three explored scenarios, indicating that the impact of turbulent shear on biofilm growth is negligible. As particle size reduces, the number of attached algae substantially differs in the laminar case compared to turbulent flow. Furthermore, a minor difference in the attached algae between the two turbulent flows is only noticeable for particle smaller than 10 μ m. These results suggest that the number of attached algae and, consequently, the biofouled particle settling velocity are not affected by the choice of turbulent shear model. Moreover, the intermittency of turbulent dissipation does not substantially influence the vertical motion of a particle.

To further investigate the influence of turbulence on the biofouling rate, we analyze the individual contributions of each term in Eq. (11). The mean contributions from collision, growth, mortality, and respiration terms towards the biofouling rate during the final 10 days of the simulation are shown in Fig. 3 for LDPE particles of size 1 mm (a), 0.1 mm (b), 10 μ m (c), and 1 μ m (d). For comparison, the average trajectory for particles with the same size is displayed in Fig. 4. The data were generated using the detailed model of Pope and Chen for the turbulent shear contribution. For a particle size of 1 mm, the growth, mortality, and respiration terms are of comparable magnitudes, with numerical values of $1.4 \times 10^6 \text{ m}^{-2} \text{ s}^{-1}$, $1.0 \times 10^6 \text{ m}^{-2} \text{ s}^{-1}$, and $3.5 \times 10^5 \text{ m}^{-2} \text{ s}^{-1}$, respectively. In contrast, the collision term is considerably smaller ($2.5 \times 10^3 \text{ m}^{-2} \text{ s}^{-1}$), and turbulent shear has a negligible impact on the collision term. With decreasing particle size, however, the contribution of turbulent shear to the biofouling rate increases. For 10 μ m particles, the collision and growth terms have similar magnitudes, at approximately $4.2 \text{ m}^{-2} \text{ s}^{-1}$ and $4.6 \text{ m}^{-2} \text{ s}^{-1}$, respectively, with turbulent shear ($3 \text{ m}^{-2} \text{ s}^{-1}$) accounting for a significant portion of the collision term. Nevertheless, we will show that the smallest particles essentially behave as passive tracers in turbulence with a negligible sinking velocity compared to vertical turbulent fluctuations.

In summary, while the turbulent shear contribution is smaller for the larger particles and more significant for smaller ones, it ultimately exerts only a minimal influence on the settling velocity (as shown in Fig. 2(b)). Due to these reasons, for the remainder of this manuscript, we adopt the biofouling rate derived from the average dissipation rate $\bar{\epsilon}$. This choice offers the numerical advantage, as the detailed shear model demands a stringent Δt of 1 s or below for numerical stability, which, together with evolving an additional stochastic differential equation for each particle, substantially increases the computational cost.

3.2. Particle motion

Next, we examine how turbulence affects vertical particle flow dynamics. Our simulation results show that the vertical transport of biofouled microplastic particles can be divided into three main categories based on density and size. The first regime is predominantly influenced by biofouling, while the second is governed by turbulent fluctuations. In the third regime, both biofouling and turbulence significantly shape the vertical transport of microplastic particles.

The first regime, hereafter referred to as the biofouling-dominated regime, exhibits a strong biofouling influence on the vertical transport of larger microplastic particles. Fig. 4(a) illustrates this behavior for a 1 mm LDPE particle, which displays oscillatory motion under both turbulent and laminar flow conditions. Similar oscillations have been previously highlighted by Kooi et al. (2017) and Kreczak et al. (2021). In this scenario, turbulence has two minor effects on particle settling dynamics. First, the time needed for particles to start settling (i.e., settling onset) decreases from approximately 20 days in laminar flow to about 11 days in turbulent flow (Fig. 4(a)). Second, turbulence affects the depth to which particles travel, a process governed by the diffusivity profile. For a MLD of 100 m, Fig. 4(a) shows that the particle

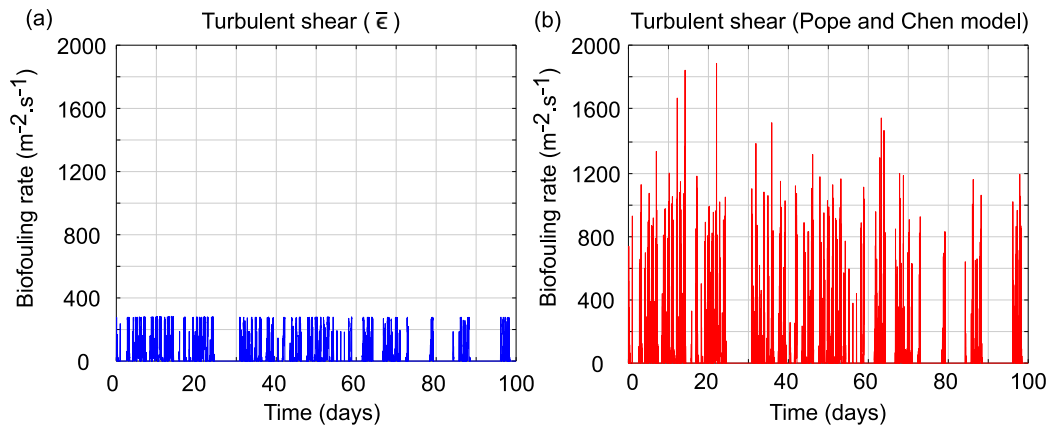


Fig. 1. The contribution from turbulent shear towards biofouling rate for a single LDPE particle of 1 μm in size using the average dissipation $\bar{\epsilon}$ (a) and the Pope and Chen model (b).

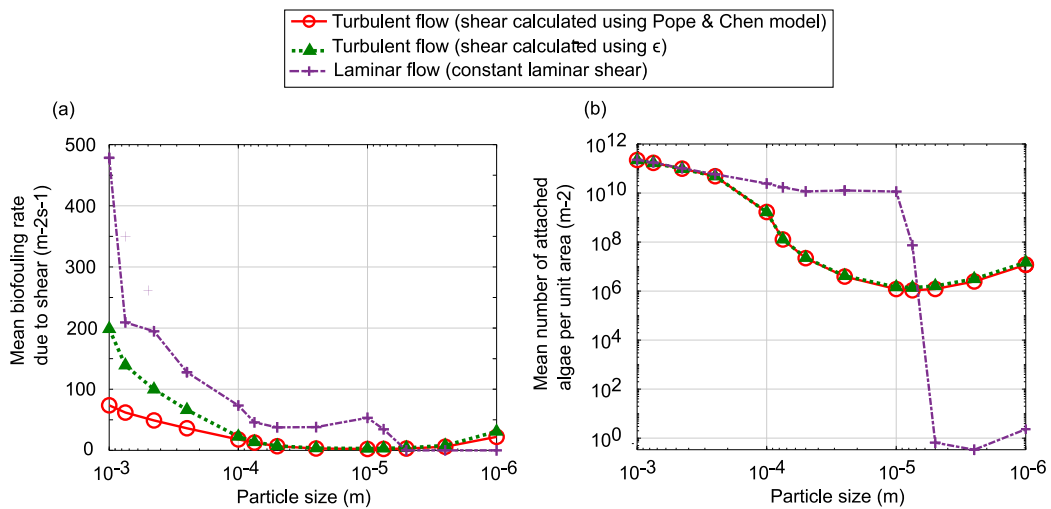


Fig. 2. (a) Mean biofouling rate due to shear and (b) mean number of attached algae per unit area for a LDPE particle of sizes ranging from 1 mm to 1 μm .

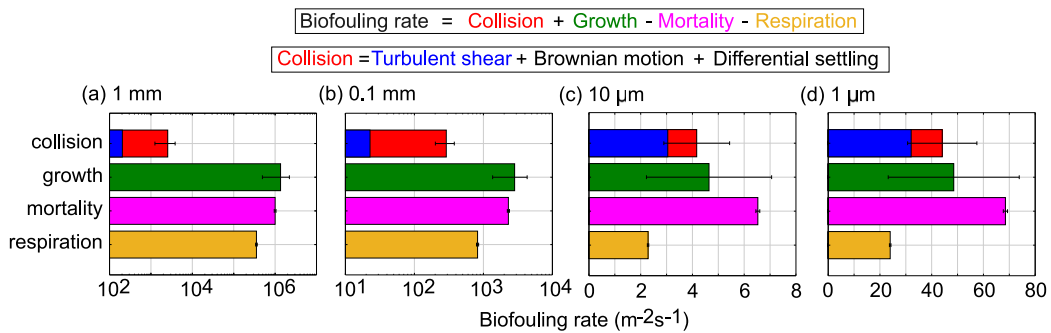


Fig. 3. The mean contributions to biofouling rate from collision, growth, mortality, and respiration observed during the last 10 days for a settling LDPE particle of (a) 1 mm (b) 0.1 mm (c) 10 μm , and (d) 1 μm in size. Error bars are provided for the different contributions.

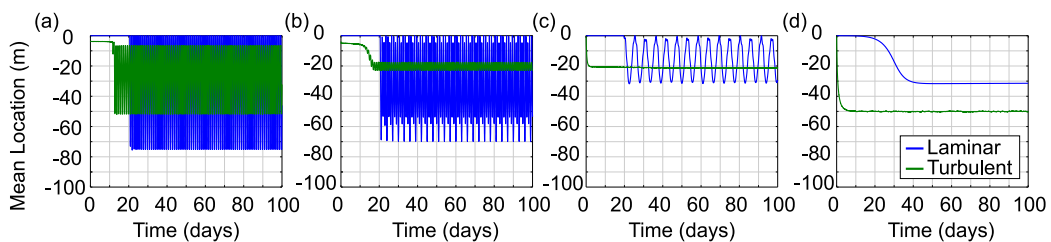


Fig. 4. Distinct behavioral patterns identified for vertical motion of biofouled microplastic particles with turbulent and laminar flow assumptions. The results shown are for LDPE with particle diameters of (a) 1 mm, (b) 0.3 mm, (c) 0.1 mm, and (d) 1 μm within a MLD of 100 m.

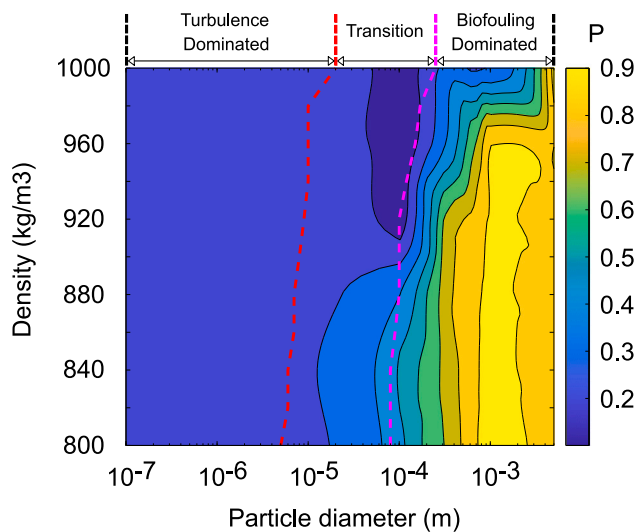


Fig. 5. Illustration of the similarity index to highlight the influence of biofouling and turbulence on a particle's vertical motion. The magenta line indicates when the oscillatory motion of particles stops, and the red line depicts when the mean particle location reaches 50 m, indicating the transition point to the turbulence-dominated regime.

descends roughly 52 m during oscillatory motion in turbulent flow, compared to 75 m in laminar flow.

In the second regime, referred to as the turbulence-dominated regime, particles follow turbulent flow paths without any contribution from biofouling and essentially behave as passive tracers. Fig. 4(d) illustrates this behavior for a particle of size 1 μm , whose mean location (or ensemble average) under turbulent conditions is approximately 50 m. This finding implies that the particles are uniformly distributed throughout the 100 m mixed layer. Our results confirm that once the particle size falls below a certain threshold, buoyant microplastic particles, regardless of plastic type, start acting similarly to tracers following flow trajectories with negligible settling velocities and, ultimately, unaffected by biofouling.

The third and final regime, hereafter referred to as the transition regime, shows contributions from biofouling and turbulence on particle transport (Figs. 4(b) and 4(c)). As particle size decreases from the biofouling-dominated regime, the oscillation window narrows, and the particles cover a smaller distance during each oscillation. With further reductions in particle size, the oscillation ceases, and the particles start to disperse throughout the water column. However, unlike the turbulence-dominated regime, the mean depth remains closer to the surface, rather than at 50 m, as illustrated in Fig. 4(c). Although the particles distribute across the water column, a greater proportion remains near the ocean surface. As the particle size continues to decline, the mean particle location gradually shifts downward until reaching the critical depth of 50 m, which indicates the onset of the turbulence-dominated regime.

We define P to quantify the respective impact of biofouling and turbulence on a particle's vertical motion. Specifically, we compare two samples of particle trajectories to measure differences in mobility arising from the addition of turbulence. A value of 1.0 for P indicates that the trajectories under turbulent and laminar flows are proportional (i.e., they exhibit a perfectly linear relationship), whereas a value of 0.0 denotes the absence of any linear relationship. Fig. 5 showcases the results of this analysis across a range of particle sizes and densities. The foremost observation is that particle size has a more significant influence on vertical motion than particle density. Particles whose motion is driven by biofouling have values above 0.5 on the similarity scale, indicated by the yellow region. This can be attributed to the high similarity between particle motion in turbulent and laminar flow,

emphasizing the negligible influence of turbulence. As the particle size reduces, P decreases, indicating differences in particle motion between turbulent and laminar flow. Fig. 5 also features two vertical lines denoting key transition points. The magenta line marks the particle size at which oscillatory motion ceases, as evidenced by Fig. 4(c). When particle size further reduces, time histories like those reported in Fig. 4(d) are obtained, with the transition to that regime indicated by the vertical red line in Fig. 5. All particle sizes smaller than this threshold belong to the turbulence-dominated regime.

Fig. 5 has significant implications for tracking the fate of microplastic particles in large-scale regional or global models. From a numerical standpoint, it is more computationally efficient to turn off the biofilm growth model for particles smaller than 10 μm , as such particles are purely convected by the underlying flow, thereby reducing computational time.

Fig. 6 further examines the distribution of particles within the ocean mixed layer by quantifying the normalized distribution of particles (N/N_0). Here, N represents the number of particles per unit depth, and N_0 quantifies the expected number of particles per unit depth to achieve a uniform distribution across the water column. Thus, $N/N_0 = 1$ indicates a uniform particle distribution. Figs. 6(b), (c), and (d), illustrate the data at the end of a 100-day period for initial particle sizes of 0.1 mm, 10 μm , and 1 μm , respectively. Meanwhile, the average location on day 100 is considered for a 1 mm particle (Figs. 6(a)), since those particles demonstrate a daily oscillatory motion.

Fig. 6(a) depicts a rise and subsequent decline in particle concentration with depth, peaking at approximately 20 m. With increasing particle density, more particles descend deeper during the oscillation process, thus reducing the number of particles concentrated at the 20 m depth. Moreover, the maximum particle concentration also exhibits a reduction as density increases, accompanied by a shift in the depth at which this accumulation occurs.

For an initial particle size of 0.1 mm (Fig. 6(b)), particle densities ranging from 800 kg/m^3 to 960 kg/m^3 exhibit an exponential decay of particle concentration with depth. As particle density increases, the number of particles closer to the ocean surface decreases, and more particles occupy deeper segments of the water column. Similar exponential decays have been reported in the field studies conducted by Kooi et al. (2016) and Reisser et al. (2015) in the North Atlantic gyre and by Brunner et al. (2015) for both the North Atlantic and North Pacific gyres. These findings emphasize the sensitivity of exponential decay patterns to variations in sea state, oceanographic profiles, particle shape, size, and density, making it difficult to directly compare with our results.

For a 1 μm particle (Fig. 6(d)), the distribution remains uniform across all particle densities, indicating that turbulent-dominated conditions have been achieved. Similar observations can be made for 10 μm particles (Fig. 6(c)), except at depths exceeding 90 m. As particle density increases, the number of particles occupying this region also rises.

3.3. Sinking characteristics

To gain further insight into the sinking characteristics of microplastic particles, we investigate two parameters: settling onset and time spent underwater. In laminar flow, we define settling onset as the moment a particle sinks below the ocean surface. Meanwhile, in turbulent flow, we define the settling onset as the moment a particle sinks below 6 m from the ocean surface. We make this distinction because the random mixed layer boundary condition induces particles to move randomly within the upper 6 m of the water column during the initial few days, as observed in Fig. 4(a).

Fig. 7 illustrates the settling onset of PP and HDPE particles in laminar and turbulent flows across various particle sizes. In laminar flow, we observe settling onsets ranging from 18 to 22 days for particles larger than 0.1 mm. As previously shown by Kooi et al. (2017), these

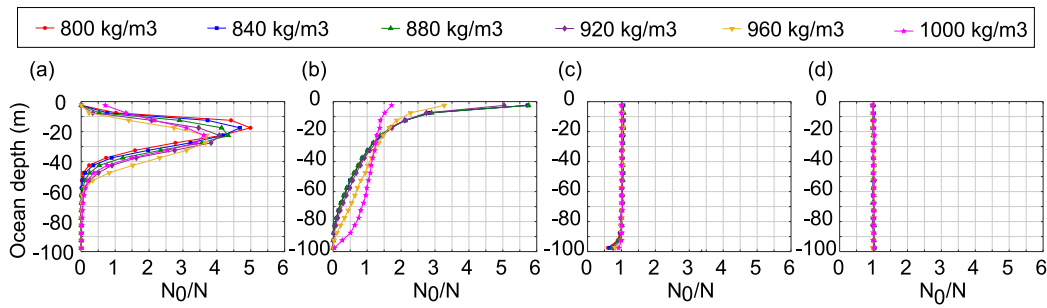


Fig. 6. Normalized distribution for the number of particles across the water column after 100 days for initial particle diameters of (a) 1 mm, (b) 0.1 mm, (c) 10 μm, and (d) 1 μm. A numerical value of 1 for N/N_0 corresponds to an even distribution of particles across the ocean depth. Results are displayed for particle densities of 800 kg/m³, 840 kg/m³, 880 kg/m³, 920 kg/m³, 960 kg/m³, 1000 kg/m³.

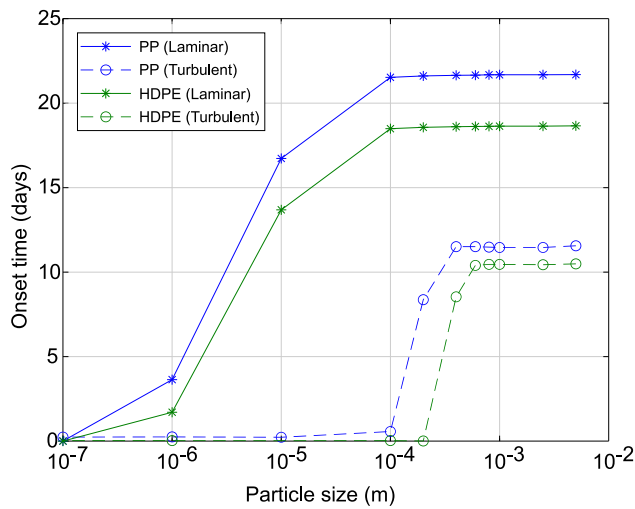


Fig. 7. Settling onset for varying particle sizes. Results are shown for PP and HDPE under turbulent and laminar flow conditions.

estimates bear similarities to the experimental findings of Fazy and Ryan (2016), who reported that the surface longevity of LDPE and HDPE microplastics with rectangular dimensions ranging from 5 mm × 5 mm × 0.1 mm to 5 mm × 5 mm × 4 mm can vary between 17 to 49 days. Conducting such experiments under turbulent conditions presents significant challenges, which our numerical model effectively overcomes. Our results show that, across all particle sizes and densities, particles initiate sinking earlier in turbulent flow compared to laminar flow. For a particle size of 1 mm, the settling onset reduces from 22 to 11 days for PP and 19 to 10 days for HDPE when turbulence is introduced. Another notable finding is that particles smaller than 0.1 mm start sinking almost immediately under turbulent conditions for both plastic types, a phenomenon the laminar flow assumption overestimates, highlighting one of the key effects of turbulence on particle settling dynamics. As the biofilm grows over time, additional velocity components from turbulence (see Eq. (4)) accelerate particle sinking relative to laminar conditions.

Fig. 8 depicts another important sinking characteristic: the total time PP and LDPE particles spend underwater, expressed as a fraction of the first 100 days. While LDPE particles, being heavier than PP, stay longer underwater, we also find that turbulence further increases the time spent underwater. The underwater residence times for turbulent and laminar flows are nearly identical in the biofouling dominant regime ($P \approx 1$). In contrast, particles smaller than 0.1 mm remain fully submerged in turbulent flow, whereas in laminar conditions, this behavior only appears at a particle size of 0.1 μm. These results indicate that turbulence is a leading factor in causing microplastic particles smaller than 0.1 mm to spend their entire lifespan underwater.

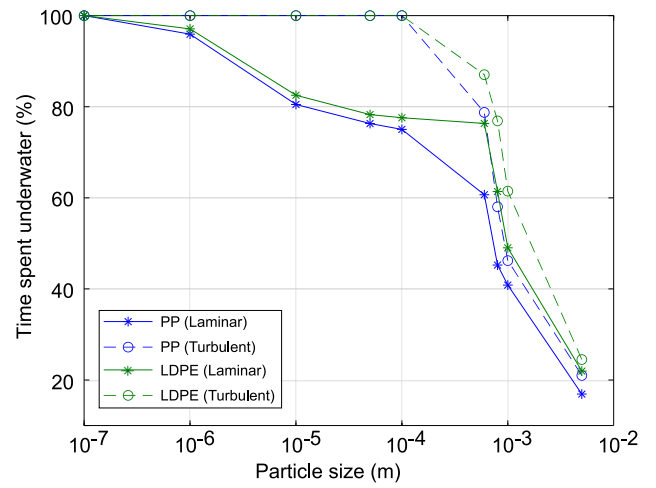


Fig. 8. The time spent by particles submerged underwater with respect to total time in the first 100 days of the simulations, expressed as a percentage. Results are shown for PP and LDPE with turbulent and laminar flow assumptions.

3.4. Particle size distribution

Finally, we examine the particle size spectra to investigate biofilm growth in a turbulent flow. Fig. S2 presents the probability density function (PDF) of normalized particle sizes ($d_{final}/d_{initial}$) after 100 days for initial sizes of 1 mm, 0.1 mm, 10 μm, and 1 μm, at densities between 800 and 1000 kg/m³. We define the particle size as the daily average, incorporating biofilm thickness. As shown in Fig. S2(a), particles initially 1 mm in diameter exhibit a Gaussian-like distribution, with the largest diameters observed at 800 kg/m³ and a mean normalized particle radius of 1.15. Increasing density reduces this normalized size. For 0.1 mm particles (Fig. S2(b)), the PDF displays a rising and declining pattern, deviating from the Gaussian symmetry observed with particles of size 1 mm. However, similar to the 1 mm case, the largest normalized particle size decreases with increasing density, meaning that the relative variations in size are less pronounced for the heaviest particles. Reducing the initial size to 10 μm sharply reduces biofilm growth, with the distribution reaching only up to 1.0005 and exhibiting a linear decline on a logarithmic scale (Fig. S2(c)). Finally, for 1 μm particles (Fig. S2(d)), the relative biofilm-induced size peaks at 1.06. These results indicate that density will not influence the final particle size distribution of microplastics when the initial size is 10 μm or smaller.

4. Conclusion

We investigated the influence of turbulence and biofouling on the vertical transport of buoyant microplastic particles in the North Pacific

Ocean. To achieve this, we developed a one-dimensional Lagrangian biophysical particle tracking model that incorporates the biofouling model of Kooi et al. (2017), adheres to the Lagrangian particle tracking guidelines of Ross and Sharples (2004), and includes additional features to accurately capture the contributions of turbulent shear to biofouling rates. Three commonly used buoyant plastic types were analyzed (PP, LDPE, HDPE) with particle sizes ranging from 5 mm to 0.1 μm . Our study focused on the mixed-layer dynamics during the first 100 days after these particles enter the ocean.

Our results show the existence of three flow regimes governing a particle's vertical motion, dictated by turbulence and biofouling. One of the major findings of this study is the particle threshold at which the transition between regimes occur for different buoyant plastic types. For PP, LDPE, and HDPE particles, the transition from the biofouling-dominated regime to the transition regime occurs at particle sizes of 0.08 mm, 0.1 mm, and 0.15 mm. Similarly, the change from the transition regime to the turbulence-dominated regime happens at 6 μm , 9 μm , and 10 μm . These results are significant because they establish the particle sizes below which buoyant microplastics can be considered as passive tracers in numerical simulations in a marine environment. Accordingly, in large-scale hydrodynamic simulations, our results show that the model used to capture the biofouling process can be deactivated in the turbulence-dominated regime to reduce computational costs.

Our findings show that depending on the particle size, turbulent shear can greatly contribute to the biofouling rate and, hence, the growth of the biofilm thickness. In the biofouling-dominated regime, turbulent shear has a negligible impact on the biofouling rate. In transition and turbulence-dominated regimes, turbulent shear plays an important role in controlling the biofouling rate. However, modeling the effects of turbulent intermittency using Pope and Chen model requires a Δt value of 1 s or lower to ensure numerical stability, which is not feasible in large-scale hydrodynamic simulations of the ocean. Furthermore, as particle size decreases, the biofilm has a negligible impact on particle motion, especially in the turbulence-dominated regime. Therefore, we recommend computing turbulent shear using the average dissipation rate $\bar{\epsilon}$ at each depth in large-scale hydrodynamic simulations, as this approach delivers sufficiently accurate results at a substantially lower computational cost. We also recommend using the Pope and Chen model for sensitivity testing and implementation with new biophysical particle tracking models, where aggregation due to turbulent shear needs to be accurately captured and a Δt value of 1 s or lower is feasible.

The Lagrangian biophysical particle tracking model developed during this numerical study offers a robust framework for analyzing how turbulence and biofouling interact to shape the vertical transport of buoyant microplastics. Given the lack of subsurface plastic concentration observations available to date, the model has the potential to identify regions where microplastics preferentially accumulate, particularly in areas with similar biological and physical characteristics. However, a limitation of this study is the exclusion of flocculation processes, which can lead to the formation of larger aggregates with higher sinking velocities altering accumulation regions (Laursen et al., 2023). Such mechanisms fall outside the scope of this research study and are recommended for future work.

CRediT authorship contribution statement

Thisal Mandula Sugathapala: Writing – review & editing, Writing – original draft, Software, Formal analysis, Conceptualization. **Tonia Capuano:** Writing – review & editing, Methodology. **Luca Brandt:** Writing – review & editing, Methodology, Funding acquisition. **Daniele Iudicone:** Writing – review & editing, Methodology, Conceptualization. **Gaetano Sardina:** Writing – review & editing, Supervision, Methodology, Funding acquisition, Conceptualization.

Declaration of competing interest

The authors declare that they have no known competing financial interests or personal relationships that could have appeared to influence the work reported in this paper.

Acknowledgments

This work is part of the international interdisciplinary project MicroplastiX (<https://www.microplastix.org/>) supported by the Joint Programming Initiative: Healthy and Productive Seas and Oceans and the governmental research council for sustainable development FORMAS, grant no. 2019 - 02172 and 2019-02173. The computations were enabled by resources provided by the National Academic Infrastructure for Supercomputing in Sweden (NAISS), partially funded by the Swedish Research Council through grant agreement no. 2022-06725.

Appendix A. Supplementary data

The model developed during this study is open-sourced and publicly available at https://github.com/thisalmandula/LPT_Biofouling_Microplastic_Turbulence.git.

Data availability

Data will be made available on request.

References

- Alosairi, Y., Al-Salem, S., Al Ragum, A., 2020. Three-dimensional numerical modelling of transport, fate and distribution of microplastics in the northwestern Arabian/Persian gulf. *Marine Poll. Bull.* 161, 111723. <http://dx.doi.org/10.1016/j.marpolbul.2020.111723>.
- Andrady, A.L., 2022. Weathering and fragmentation of plastic debris in the ocean environment. *Marine Poll. Bull.* 180, 113761. <http://dx.doi.org/10.1016/j.marpolbul.2022.113761>.
- Baas, P., de Rooode, S.R., Lenderink, G., 2008. The scaling behaviour of a turbulent kinetic energy closure model for stably stratified conditions. *Bound.-Layer Meteorol.* 127, 17–36. <http://dx.doi.org/10.1007/s10546-007-9253-y>.
- Bigdeli, M., Mohammadian, A., Pilechi, A., Taheri, M., 2022. Lagrangian modeling of marine microplastics fate and transport: The state of the science. *J. Mar. Sci. Eng.* 10 (4), <http://dx.doi.org/10.3390/jmse10040481>.
- Blanke, B., Delecluse, P., 1993. Variability of the tropical atlantic ocean simulated by a general circulation model with two different mixed-layer physics. *J. Phys. Oceanogr.* 23 (7), 1363–1388. [http://dx.doi.org/10.1175/1520-0485\(1993\)023<1363:VOTTAO>2.0.CO;2](http://dx.doi.org/10.1175/1520-0485(1993)023<1363:VOTTAO>2.0.CO;2).
- Borrelle, S., Ringma, J., Lavender Law, K., Monnahan, C., Lebreton, L., McGivern, A., Murphy, E., Jambeck, J., Leonard, G., Hilleary, M., Eriksen, M., Possingham, H., De Frond, H., Gerber, L., Polidoro, B., Tahir, A., Bernard, M., Mallos, N., Barnes, M., Rochman, C., 2020. Predicted growth in plastic waste exceeds efforts to mitigate plastic pollution. *Science* 369 (6509), 1515–1518. <http://dx.doi.org/10.1126/SCIENCE.ABA3656>.
- Bouffadel, M., Liu, R., Zhao, L., Lu, Y., Özgökmen, T., Nedwed, T., Lee, K., 2020. Transport of oil droplets in the upper ocean: Impact of the eddy diffusivity. *J. Geophys. Res. Ocean.* 125 (2), <http://dx.doi.org/10.1029/2019JC015727>.
- Brunner, K., Kukulka, T., Proskurowski, G., Law, K.L., 2015. Passive buoyant tracers in the ocean surface boundary layer: 2. observations and simulations of microplastic marine debris. *J. Geophys. Res. Ocean.* 120 (11), 7559–7573. <http://dx.doi.org/10.1002/2015JC010840>.
- Burd, A.B., Jackson, G.A., 2009. Particle aggregation. *Annu. Rev. Mar. Sci.* 1 (1), 65–90. <http://dx.doi.org/10.1146/annurev.marine.010908.163904>.
- Canuto, V.M., Howard, A., Cheng, Y., Dubovikov, M.S., 2001. Ocean turbulence. part i: One-point closure model—momentum and heat vertical diffusivities. *J. Phys. Oceanogr.* 31 (6), 1413–1426. [http://dx.doi.org/10.1175/1520-0485\(2001\)031<1413:OTPIOP>2.0.CO;2](http://dx.doi.org/10.1175/1520-0485(2001)031<1413:OTPIOP>2.0.CO;2).
- Capuano, T.A., Botte, V., Sardina, G., Brandt, L., Grujić, A., Iudicone, D., 2024. Oceanic realistic application of a microplastic biofouling model to the river discharge case. *Environ. Pollut.* 359, 124501. <http://dx.doi.org/10.1016/j.envpol.2024.124501>.
- Cole, M., Lindeque, P., Halsband, C., Galloway, T.S., 2011. Microplastics as contaminants in the marine environment: A review. *Marine Poll. Bull.* 62 (12), 2588–2597. <http://dx.doi.org/10.1016/j.marpolbul.2011.09.025>.

- Cózar, A., Echevarría, F., González-Gordillo, J.I., Irigoien, X., Úbeda, B., Hernández-León, S., Palma, Álvaro T., Navarro, S., de Lomas, J.G., Ruiz, A., de Puellas, M.L.F., Duarte, C.M., 2014. Plastic debris in the open ocean. *Proc. Natl. Acad. Sci.* 111 (28), 10239–10244. <http://dx.doi.org/10.1073/pnas.1314705111>.
- Daily, J., Hoffman, M.J., 2020. Modeling the three-dimensional transport and distribution of multiple microplastic polymer types in lake erie. *Marine Poll. Bull.* 154, 111024. <http://dx.doi.org/10.1016/j.marpolbul.2020.111024>.
- Deardorff, J.W., 1980. Stratocumulus-capped mixed layers derived from a three-dimensional model. *Bound.-Layer Meteorol.* 18, 495–527. <http://dx.doi.org/10.1007/BF00119502>.
- Dietrich, W.E., 1982. Settling velocity of natural particles. *Water Resour. Res.* 18 (6), 1615–1626. <http://dx.doi.org/10.1029/WR018i006p01615>.
- Fazey, F.M., Ryan, P.G., 2016. Biofouling on buoyant marine plastics: An experimental study into the effect of size on surface longevity. *Environ. Pollut.* 210, 354–360. <http://dx.doi.org/10.1016/j.envpol.2016.01.026>.
- Fischer, R., Lobelle, D., Kooi, M., Koelmans, A.A., Onink, V., Laufkötter, C., Amaral-Zettler, L., Yool, A., van Sebille, E., 2022. Modelling submerged biofouled microplastics and their vertical trajectories. *Biogeosciences* 19 (8), 2211–2234. <http://dx.doi.org/10.5194/bg-19-2211-2022>.
- Francalanci, S., Paris, E., Solari, L., 2021. On the prediction of settling velocity for plastic particles of different shapes. *Environ. Pollut.* 290, 118068. <http://dx.doi.org/10.1016/j.envpol.2021.118068>.
- Gaspar, P., Grégoris, Y., Lefevre, J.-M., 1990. A simple eddy kinetic energy model for simulations of the oceanic vertical mixing: Tests at station papa and long-term upper ocean study site. *J. Geophys. Res. Ocean.* 95 (C9), 16179–16193. <http://dx.doi.org/10.1029/JC095iC09p16179>.
- Hidalgo-Ruz, V., Gutow, L., Thompson, R.C., Thiel, M., 2012. Microplastics in the marine environment: A review of the methods used for identification and quantification. *Environ. Sci. Technol.* 46 (6), 3060–3075. <http://dx.doi.org/10.1021/es2031505>.
- Hunter, J., 1987. The application of lagrangian particle-tracking techniques to modelling of dispersion in the sea. In: *Numerical Modelling: Applications To Marine Systems*. In: North-Holland Mathematics Studies, vol. 145, North-Holland, pp. 257–269. [http://dx.doi.org/10.1016/S0304-0208\(08\)70037-9](http://dx.doi.org/10.1016/S0304-0208(08)70037-9).
- Hunter, J., Craig, P., Phillips, H., 1993. On the use of random walk models with spatially variable diffusivity. *J. Comput. Phys.* 106 (2), 366–376. [http://dx.doi.org/10.1016/S0021-9991\(83\)71114-9](http://dx.doi.org/10.1016/S0021-9991(83)71114-9).
- Isern-Fontanet, J., Turiel, A., 2021. On the connection between intermittency and dissipation in ocean turbulence: A multifractal approach. *J. Phys. Oceanogr.* 51 (8), 2639–2653. <http://dx.doi.org/10.1175/JPO-D-20-0256.1>.
- Iwasaki, S., Isobe, A., Kako, S., Uchida, K., Tokai, T., 2017. Fate of microplastics and mesoplastics carried by surface currents and wind waves: A numerical model approach in the sea of Japan. *Marine Poll. Bull.* 121 (1), 85–96. <http://dx.doi.org/10.1016/j.marpolbul.2017.05.057>.
- Jalón-Rojas, I., Wang, X.H., Fredj, E., 2019. A 3d numerical model to track marine plastic debris (trackmpd): Sensitivity of microplastic trajectories and fates to particle dynamical properties and physical processes. *Marine Poll. Bull.* 141, 256–272. <http://dx.doi.org/10.1016/j.marpolbul.2019.02.052>.
- Kaiser, D., Kowalski, N., Waniek, J.J., 2017. Effects of biofouling on the sinking behavior of microplastics. *Environ. Res. Lett.* 12, 124003. <http://dx.doi.org/10.1088/1748-9326/aa8e8b>.
- Kooi, M., Nes, E.H.v., Scheffer, M., Koelmans, A.A., 2017. Ups and downs in the ocean: Effects of biofouling on vertical transport of microplastics. *Environ. Sci. Technol.* 51 (14), 7963–7971. <http://dx.doi.org/10.1021/acs.est.6b04702>.
- Kooi, M., Reisser, J., Slat, B., Ferrari, F.F., Schmid, M.S., Cunsolo, S., Brambini, R., Noble, K., Sirks, L.-A., Linders, T.E.W., Schoeneich-Argent, R.I., Koelmans, A.A., 2016. The effect of particle properties on the depth profile of buoyant plastics in the ocean. *Sci. Rep.* 6, 33882. <http://dx.doi.org/10.1038/srep33882>.
- Kreczak, H., Willmott, A.J., Baggaley, A.W., 2021. Subsurface dynamics of buoyant microplastics subject to algal biofouling. *Limnol. Oceanogr.* 66 (9), 3287–3299. <http://dx.doi.org/10.1002/lno.11879>.
- Lamorgese, A.G., Pope, S.B., Yeung, P.K., Sawford, B.L., 2007. A conditionally cubic-gaussian stochastic lagrangian model for acceleration in isotropic turbulence. *J. Fluid Mech.* 582, 423–448. <http://dx.doi.org/10.1017/S0022112007006052>.
- Laursen, S.N., Fruergaard, M., Dodhia, M.S., Posth, N.R., Rasmussen, M.B., Larsen, M.N., Shilla, D., Shilla, D., Kilawe, J.J., Kizenga, H.J., Andersen, T.J., 2023. Settling of buoyant microplastic in estuaries: The importance of flocculation. *Sci. Total Environ.* 886, 163976. <http://dx.doi.org/10.1016/j.scitotenv.2023.163976>.
- Li, S., Ding, F., Flury, M., Wang, J., 2023. Dynamics of macroplastics and microplastics formed by biodegradable mulch film in an agricultural field. *Sci. Total Environ.* 894, 164674. <http://dx.doi.org/10.1016/j.scitotenv.2023.164674>.
- Liubartseva, S., Coppini, G., Lecci, R., Clementi, E., 2018. Tracking plastics in the mediterranean: 2d lagrangian model. *Marine Poll. Bull.* 129 (1), 151–162. <http://dx.doi.org/10.1016/j.marpolbul.2018.02.019>.
- Lobelle, D., Kooi, M., Koelmans, A.A., Laufkötter, C., Jongedijk, C.E., Kehl, C., van Sebille, E., 2021. Global modeled sinking characteristics of biofouled microplastic. *J. Geophys. Res. Ocean.* 126 (4), <http://dx.doi.org/10.1029/2020JC017098>.
- Mansui, J., Molcard, A., Ourmières, Y., 2015. Modelling the transport and accumulation of floating marine debris in the mediterranean basin. *Marine Poll. Bull.* 91 (1), 249–257. <http://dx.doi.org/10.1016/j.marpolbul.2014.11.037>.
- Osborn, T.R., 1980. Estimates of the local rate of vertical diffusion from dissipation measurements. *J. Phys. Oceanogr.* 10 (1), 83–89. [http://dx.doi.org/10.1175/1520-0485\(1980\)10<0083:EOTLRO>2.0.CO;2](http://dx.doi.org/10.1175/1520-0485(1980)10<0083:EOTLRO>2.0.CO;2).
- Pearson, B., Fox-Kemper, B., 2018. Log-normal turbulence dissipation in global ocean models. *Phys. Rev. Lett.* 120, 094501. <http://dx.doi.org/10.1103/PhysRevLett.120.094501>.
- Peters, H., Gregg, M., 1988. Some dynamical and statistical properties of equatorial turbulence. In: Nihou, J., Jamart, B. (Eds.), *Small-Scale Turbulence and Mixing in the Ocean*. In: Elsevier Oceanography Series, vol. 46, Elsevier, pp. 185–200. [http://dx.doi.org/10.1016/S0422-9894\(08\)70546-4](http://dx.doi.org/10.1016/S0422-9894(08)70546-4).
- Pilechi, A., Mohammadian, A., Murphy, E., 2022. A numerical framework for modeling fate and transport of microplastics in inland and coastal waters. *Marine Poll. Bull.* 184, 114119. <http://dx.doi.org/10.1016/j.marpolbul.2022.114119>.
- Plastic Europe, 2022. *Plastics-the facts 2022*.
- Pope, S.B., 2000. *Turbulent Flows*. Cambridge University Press, <http://dx.doi.org/10.1017/CBO9780511840531>.
- Pope, S.B., Chen, Y.L., 1990. The velocity-dissipation probability density function model for turbulent flows. *Phys. Fluids A: Fluid Dyn.* 2 (8), 1437–1449. <http://dx.doi.org/10.1063/1.857592>.
- Potemra, J.T., 2012. Numerical modeling with application to tracking marine debris. *Marine Poll. Bull.* 65 (1), 42–50. <http://dx.doi.org/10.1016/j.marpolbul.2011.06.026>.
- Reisser, J., Slat, B., Noble, K., du Plessis, K., Epp, M., Proietti, M., de Sonnevill, J., Becker, T., Pattiaratchi, C., 2015. The vertical distribution of buoyant plastics at sea: an observational study in the north atlantic gyre. *Biogeosciences* 12 (4), 1249–1256. <http://dx.doi.org/10.5194/bg-12-1249-2015>.
- Ross, O.N., Sharples, J., 2004. Recipe for 1-d lagrangian particle tracking models in space-varying diffusivity. *Limnol. Oceanography: Methods* 2 (9), 289–302. <http://dx.doi.org/10.4319/lom.2004.2.289>.
- Shamskhany, A., Karimpour, S., 2022. The role of microplastics' size and density on their vertical turbulent mixing and transport. In: *Proceedings of the Canadian Society of Civil Engineering Annual Conference 2021*. Springer Nature Singapore, Singapore, pp. 253–265.
- Thorpe, S.A., 2005. *The Turbulent Ocean*. Cambridge University Press, <http://dx.doi.org/10.1017/CBO9780511819933>.
- Thorpe, S.A., 2007. *An Introduction to Ocean Turbulence*. Cambridge University Press, <http://dx.doi.org/10.1017/CBO9780511801198>.
- United Nations Environment Programme, 2021. *Drowning in plastics - marine litter and plastic waste vital graphics*.
- Van Melkebeke, M., Janssen, C., De Meester, S., 2020. Characteristics and sinking behavior of typical microplastics including the potential effect of biofouling: Implications for remediation. *Environ. Sci. Technol.* 54 (14), 8668–8680. <http://dx.doi.org/10.1021/acs.est.9b07378>.
- van Sebille, E., Griffies, S.M., Abernathy, R., Adams, T.P., Berloff, P., Biastoch, A., Blanke, B., Chassignet, E.P., Cheng, Y., Cotter, C.J., Deleersnijder, E., Döös, K., Drake, H.F., Drijfhout, S., Gary, S.F., Heemink, A.W., Kjellsson, J., Koszalka, I.M., Lange, M., Lique, C., MacGilchrist, G.A., Marsh, R., Mayorga Adame, C.G., McAdam, R., Nencioli, F., Paris, C.B., Piggott, M.D., Polton, J.A., Rühls, S., Shah, S.H., Thomas, M.D., Wang, J., Wolfram, P.J., Zanna, L., Zika, J.D., 2018. Lagrangian ocean analysis: Fundamentals and practices. *Ocean. Model.* 121, 49–75. <http://dx.doi.org/10.1016/j.ocemod.2017.11.008>.
- Visser, A.W., 1997. Using random walk models to simulate the vertical distribution of particles in a turbulent water column. *Mar. Ecol. Prog. Ser.* 158, 275–281.
- Watteaux, R., Sardina, G., Brandt, L., Iudicone, D., 2019. On the time scales and structure of lagrangian intermittency in homogeneous isotropic turbulence. *J. Fluid Mech.* 867, 438–481. <http://dx.doi.org/10.1017/jfm.2019.127>.
- Whalen, C.B., 2021. Best practices for comparing ocean turbulence measurements across spatiotemporal scales. *J. Atmos. Ocean. Technol.* 38 (4), 837–841. <http://dx.doi.org/10.1175/JTECH-D-20-0175.1>.
- Xue, P., Schwab, D.J., Zhou, X., Huang, C., Kibler, R., Ye, X., 2018. A hybrid Lagrangian-Eulerian particle model for ecosystem simulation. *J. Mar. Sci. Eng.* 6 (4), <http://dx.doi.org/10.3390/jmse6040109>.
- Yeung, P.K., Pope, S.B., Lamorgese, A.G., Donzis, D.A., 2006. Acceleration and dissipation statistics of numerically simulated isotropic turbulence. *Phys. Fluids* 18 (6), 065103. <http://dx.doi.org/10.1063/1.2204053>.
- Zhang, H., 2017. Transport of microplastics in coastal seas. *Estuar. Coast. Shelf Sci.* 199, 74–86. <http://dx.doi.org/10.1016/j.ecss.2017.09.032>.
- Zhao, D., Li, M., 2019. Dependence of wind stress across an air-sea interface on wave states. *J. Ocean.* 75 (3), 207–223. <http://dx.doi.org/10.1007/s10872-018-0494-9>.